Journal of Sound and Vibration 549 (2023) 117574

Contents lists available at ScienceDirect

Journal of Sound and Vibration

journal homepage: www.elsevier.com/locate/jsvi

Modal analysis through response-based FRFs: Additional modes for local diagnoses

Simone De Carolis [a,*], Arcangelo Messina [b], Leonardo Soria [a]

[a] Dipartimento di Meccanica, Matematica e Management, Politecnico di Bari, Bari, Italy
[b] Dipartimento di Ingegneria dell'Innovazione, Università del Salento, Lecce, Italy

ARTICLE INFO

MSC:
00-01
99-00

Keywords:
R-FRFs
Transmissibility
Damage detection
SHM
Experimental modal analysis

ABSTRACT

The importance and role of a specific class of global transmissibility matrices (global TFs), here named response-based frequency response functions (R-FRFs), in the areas of the identification and continuous monitoring of structures, is discussed and expanded in the present paper. The R-FRFs, as specialized frequency response functions, have been recently introduced in the literature, and, as originally proved, they are able to inherently provide local poles related to the system under investigation, but, virtually, with a different set of boundary conditions; i.e. as if some of the original degrees of freedom, arbitrarily chosen by the analyst, were constrained to ground. In this paper, such a concept is extended, including mode shapes. Herein, we show that the R-FRFs are also able to provide local modes associated with the aforementioned local poles. In this regard, we provide a parametric model of the R-FRFs matrix, suitable for being tackled through frequency-domain estimators from the field of experimental and operational modal analysis, which let these additional modal parameters to be identified. Such a conceptual extension is carried out by both a theoretical and a numerical point of view. We process data sets from numerical and real-world experimental case studies and discuss the corresponding results. The estimated poles and modes are employed to detect structural modifications, in turn confirming the significance of response-based frequency response functions in the field of damage detection and structural health monitoring (SHM).

1. Introduction

Many different modal analysis based protocols have been developed over the last four decades in the area of system dynamics with unconnected aims, from model updating to diagnostics. With regards to only the last-mentioned, also commonly named structural health monitoring (SHM) or damage detection, an extraordinarily important number of research efforts have been made available. Therefore, a possible lack of citations is only due to mere reasons of brevity, rather than to relevance or irrelevance with respect to the content presented in this paper.

A reasonable citation base could be found, for example, in Refs. [1–5], where devices, physical quantities, methods and perspectives involved in the numerous numerical and/or experimental protocols proposed in the scientific literature are illustrated and discussed. Devices comprise all possible transducers (typically, but not exhaustively, accelerometers and load cells) and the relevant conditioning systems followed by A/D digital boards. Transfer functions appear to be the most representative and commonly adopted physical quantities, computed by measurements' processing, and, specifically, frequency response functions (FRFs), generally in the form of the ratios between forces and output accelerations (accelerances or apparent masses). However,

* Corresponding author.
E-mail address: simone.decarolis@poliba.it (S. De Carolis).

https://doi.org/10.1016/j.jsv.2023.117574
Received 15 July 2022; Received in revised form 4 December 2022; Accepted 21 January 2023
Available online 21 January 2023

FRFs could be seen from a wider perspective as functions relating different outputs of a linear time-invariant system. In such a latter perspective, during the last two decades, researchers have started investigating transmissibility functions (see e.g. [6–13]). In particular, Ribeiro [6] generalized a transmissibility concept from one degree of freedom systems to structures with multiple degrees of freedom. Specifically, he obtained a relationship between vectors of unknown responses and measurable responses, along with a pseudo-inversion when certain conditions between the number of considered responses (known/measured and unknown) are not fulfilled. Through his theoretical analyses, Ribeiro introduced a new concept that seemed to be promising not only as a monitoring tool, but even for its predictive capability. The results of this effort were also extended to a wider audience two years later (see Ribeiro et al. [8]). Sampaio et al. [7], used the transmissibility concept in the area of damage detection. They noticed that more research efforts would have been needed to better understand and explore all the possible improvements in the usage of the technique. With regard to this topic, other interesting contributions [7,10,11,13] have been produced in the following years. Maia et al. [9] presented a general overview of the transmissibility concept, pros and cons, and possible applications; they also recognized that no simple relationships (if any) could be established between peaks and anti-peaks of transmissibility functions and FRFs. The recent paper from Yan et al. [12] certainly testifies the great interest in transmissibility-based system identification, in the area of structural health monitoring, by discussing existing studies dealing with the concept and the usage of transmissibility functions; they specifically conclude that proving the capabilities of employing transmissibilities in an unsupervised manner, in the field of damage localization, might be tough.

Independently of the previously cited works, Messina [14] followed a different formal approach for defining a new class of transmissibility functions (the R-FRFs), specifically designed to enrich the intrinsic modal database of the system under study and to allow analyzing the system in a local sense. In fact, R-FRFs provide poles of the original structure when some of its degrees of freedom are, virtually, considered constrained to the ground; thus, such a local sense is achieved when one virtually hampers the vibration of a specific part of the structure, but letting the remaining (and local) part to freely vibrate. The possibility of adding those new poles comes from the fact that they are inherently related to the original system, even though it is considered partially and virtually constrained. In this context, “virtually” means that no physical locks are actually needed to be added, whilst new boundary conditions are obtained simply by measuring the R-FRFs, through performing a feasible and attractive experimental procedure, aimed at investigating local structural modifications, potentially occurring on the system. Such a dual nature (of being local and additional) of the poles identifiable from R-FRFs, is theoretically and experimentally proved in Refs. [14,15], respectively. The results of the investigations carried out in the cited efforts encouraged the research group to implement techniques aimed at improving the estimation process of R-FRFs from experimental data [16], whilst, in the present paper, we identify poles and the corresponding mode shapes, to be intended as local and additional modal parameters. Basically, we here extend the application of curve fitting methods, classically used in the cases of experimental modal analysis (EMA) and operational modal analysis (OMA), to that of R-FRFs, whose parametric model is derived in terms of perturbated original system’s modal parameters, combined with matrices whose entries are transmission elements in the form of combinations of physical lumped parameters relating defined groups of degrees of freedom. Usually, transmissibility-driven stochastic identification techniques [17,18] elaborate scalar transmissibility measurements, retrieved over different loading conditions, in order to obtain rational functions with poles equal to those of the original system. Specifically, in [19] poly-reference transmissibility-based OMA, uninfluenced by the content of the input spectrum, is introduced by proposing a parametric model of the transmissibility functions exploited by an identification approach that only captures the eigenstructure of the system of interest. Similarly, in [20] multivariable transmissibilities, also known as global TFs, are related to scalar transmissibilities to obtain pseudo scalar transmissibility functions, which system poles can be extracted from. In the present work, we provide a parametric model of R-FRFs, as a specific class of global TFs, showing how these functions comprise additional local modal parameters. Such an objective is worth to be pursued, since structural modifications or damage, occurring in specific locations of the system under test, often need processing of both modal parameter kinds, that is poles and modes.

The rest of the paper is organized as follows. In Section 2, we derive the modal partial fraction decomposition of R-FRFs for a linear time-invariant system, containing the additional/local poles and mode shapes. In Section 3, we develop a specialized algorithm to identify such additional/local poles and modes. In Section 4, we exploit numerical and experimental case studies; the former is used to evaluate the performance of the obtained algorithm on differently estimated R-FRFs, by comparing the computed modal parameters; the latter allows for performing a full damage detection analysis of a slender beam, to elucidate and highlight the additional/local nature of modal parameters extracted by R-FRFs’ estimates. Finally, in Section 5, we summarize the main conclusions of this work. Moreover, in Appendix, we propose an alternative theoretical approach to obtain the modal partial fraction decomposition of R-FRFs, which we compare with that derived in Section 2.

2. R-FRFs’ modal model

We consider a linear, time-invariant, damped vibrating system having N degrees of freedom (dofs), for which the well-known input–output relationship, in the Laplace domain s, from rest initial conditions, is

$$\mathbf{B}(s)\mathbf{X}(s) = \mathbf{F}(s), \tag{1}$$

where the dynamic stiffness matrix $\mathbf{B}(s)$, and the displacement $\mathbf{X}(s)$ and force $\mathbf{F}(s)$ vectors can be partitioned as

$$\left[\begin{array}{c|c} \mathbf{B}_{11}(s)_{n\times n} & \mathbf{B}_{12}(s)_{n\times m} \\ \hline \mathbf{B}_{21}(s)_{m\times n} & \mathbf{B}_{22}(s)_{m\times m} \end{array}\right] \left(\begin{array}{c} \mathbf{Z}(s)_{n\times 1} \\ \hline \mathbf{Y}(s)_{m\times 1} \end{array}\right) = \left(\begin{array}{c} \mathbf{Q}(s)_{n\times 1} \\ \hline \mathbf{0}_{m\times 1} \end{array}\right). \tag{2}$$

We assume that the displacement vector $\mathbf{Z}(s)$ includes the n output response dofs in which the input forces, described by the vector $\mathbf{Q}(s)$, are applied. We define such dofs as forced or driving, whilst the $\mathbf{Y}(s)$ vector contains the output displacements of the $m = N-n$ unforced dofs, here referred to as guided or free.

A linear output–output relationship is obtained by extracting the latter m equations related to free dofs' motions in Eq. (2):

$$\mathbf{Y}(s) = -\mathbf{B}_{22}^{-1}(s)\mathbf{B}_{21}(s)\mathbf{Z}(s) = \mathbf{R}(s)\mathbf{Z}(s), \tag{3}$$

where the matrix $\mathbf{R}(s)$ is expressed in terms of the dynamic stiffness partitions and represents a $m \times n$ response-based transfer function matrix connecting driving and free dofs. Focusing on the first partition $\mathbf{B}_{22}^{-1}(s)$, we notice that it represents the transfer function matrix $\mathbf{H}_g(s)$ of what we call the "virtually grounded system". It arises from partitioning the original dynamic stiffness $\mathbf{B}(s)$ and takes the physical meaning of the original system, characterized by the transfer matrix $\mathbf{H}(s) = \mathbf{B}^{-1}(s)$, subjected to virtually locking constraints on the m driving dofs $\mathbf{Z}(s)$ [14].

In fact, by rephrasing Eq. (3) in the following form

$$\mathbf{Y}(s) = \mathbf{B}_{22}^{-1}(s)\mathbf{F}_{eq}(s) = \mathbf{H}_g(s)\mathbf{F}_{eq}(s), \tag{4}$$

where $\mathbf{F}_{eq}(s) = -\mathbf{B}_{21}(s)\mathbf{Z}(s)$ is a $m \times 1$ vector containing the restoring forces, induced by the motion of the n driving dofs, which cause the free dofs' displacements $\mathbf{Y}(s)$ and related to elements connecting the two groups of dofs as indicated by the partition $\mathbf{B}_{21}(s)$. We interpret the forces $\mathbf{F}_{eq}(s)$ as the equivalent forces that one should apply to the n free dofs' locations of the original system, when subjected to the virtual boundary constraints $\mathbf{Z}(s) = \mathbf{0}$.

From the modal analysis theory, by considering the general case of underdamped real-world systems, containing passive damping mechanisms [21], $\mathbf{H}_g(s)$ can be modally decomposed as

$$\mathbf{H}_g(s) = \sum_{r=1}^{N_p}\left(\frac{\boldsymbol{\psi}_r \boldsymbol{L}_r^{\mathrm{T}}}{s-\lambda_r} + \frac{\boldsymbol{\psi}_r^* \boldsymbol{L}_r^{\mathrm{H}}}{s-\lambda_r^*}\right) = \sum_{r=1}^{2N_p}\left(\frac{\boldsymbol{\psi}_r \boldsymbol{L}_r^{\mathrm{T}}}{s-\lambda_r}\right), \tag{5}$$

with

$$\lambda_r = -\zeta_r\omega_{u_r} + \mathrm{i}\omega_{u_r}\sqrt{1-\zeta_r^2}, \tag{6}$$

where $(.)^{\mathrm{H}}$ indicates Hermitian transposition, $(.)^*$ denotes complex conjugation, N_p is the number of modes, λ_r are the complex valued roots, appearing in complex conjugate pairs, of the system characteristic equation $|\mathbf{B}_{22}(s)| = 0$ with ω_{u_r} the undamped natural frequency and ζ_r the damping ratio, $\boldsymbol{\psi}_r$ are the mode shape vectors and $\boldsymbol{L}_r$ are the so-called modal participation vectors. These additional poles and modes, belonging to the virtually grounded system, are included in the matrix $\mathbf{R}(s)$ that, in turn, can be classified as a response-based transfer matrix. Actually, $\mathbf{R}(s)$ is obtained by multiplying the transfer matrix in Eq. (5) by the partition $\mathbf{B}_{21}(s)$, which can be expressed as

$$\mathbf{B}_{21}(s) = s^2\mathbf{M}_{21} + s\mathbf{C}_{21} + \mathbf{K}_{21}, \tag{7}$$

where $\mathbf{M}_{21}$, $\mathbf{C}_{21}$ and $\mathbf{K}_{21}$ describe the mass, damping, and stiffness matrix relations between the two subsets of responses $\mathbf{Y}$ and $\mathbf{Z}$ that we call transmission elements. Rewriting the $m \times n$ matrix $\mathbf{R}(s)$ in terms of the virtually grounded system modal parameters in Eq. (5) and of the transmission elements in Eq. (7), we obtain

$$\mathbf{R}(s) = \sum_{r=1}^{2N_p}\left(-\frac{\boldsymbol{\psi}_r \boldsymbol{L}_r^{\mathrm{T}} s^2\mathbf{M}_{21}}{s-\lambda_r} - \frac{\boldsymbol{\psi}_r \boldsymbol{L}_r^{\mathrm{T}} s\mathbf{C}_{21}}{s-\lambda_r} - \frac{\boldsymbol{\psi}_r \boldsymbol{L}_r^{\mathrm{T}}\mathbf{K}_{21}}{s-\lambda_r}\right). \tag{8}$$

By accounting for the following identities

$$\frac{s^2}{s-\lambda_r} - s - \lambda_r = \mathcal{L}\left(\frac{d^2\mathrm{e}^{\lambda_r\tau}}{d\tau^2}\right) = \mathcal{L}\left(\lambda_r^2\mathrm{e}^{\lambda_r\tau}\right) = \frac{\lambda_r^2}{s-\lambda_r}, \tag{9}$$

$$\frac{s}{s-\lambda_r} - 1 = \mathcal{L}\left(\frac{d\mathrm{e}^{\lambda_r\tau}}{d\tau}\right) = \mathcal{L}\left(\lambda_r\mathrm{e}^{\lambda_r\tau}\right) = \frac{\lambda_r}{s-\lambda_r}, \tag{10}$$

where $\mathcal{L}(.)$ indicates the Laplace transformation, $\frac{d(.)}{d\tau}$ and $\frac{d^2(.)}{d\tau^2}$ the first and second derivative with respect to the time variable τ, and $\mathrm{e}^{(.)}$ is the exponential function, we rewrite Eq. (8) as

$$\begin{aligned}\mathbf{R}(s) = &\sum_{r=1}^{2N_p}\left(\frac{\boldsymbol{\psi}_r \boldsymbol{L}_r^{\mathrm{T}}\left(-\lambda_r^2\mathbf{M}_{21} - \lambda_r\mathbf{C}_{21} - \mathbf{K}_{21}\right)}{s-\lambda_r}\right) + \\ &- s\left(\sum_{r=1}^{2N_p}\boldsymbol{\psi}_r \boldsymbol{L}_r^{\mathrm{T}}\right)\mathbf{M}_{21} - \left(\sum_{r=1}^{2N_p}\lambda_r\boldsymbol{\psi}_r \boldsymbol{L}_r^{\mathrm{T}}\right)\mathbf{M}_{21} - \left(\sum_{r=1}^{2N_p}\boldsymbol{\psi}_r \boldsymbol{L}_r^{\mathrm{T}}\right)\mathbf{C}_{21}.\end{aligned} \tag{11}$$

By, moreover, inverse Laplace transforming Eq. (5), we obtain the so-called impulse response function (IRF) matrix

$$\mathbf{h}_g(\tau) = \sum_{r=1}^{2N_p}\boldsymbol{\psi}_r \boldsymbol{L}_r^{\mathrm{T}}\mathrm{e}^{\lambda_r\tau}, \tag{12}$$

whose first derivative is

$$\dot{\mathbf{h}}_g(\tau) = \sum_{r=1}^{2N_p} \boldsymbol{\psi}_r \boldsymbol{L}_r^{\mathrm{T}} \lambda_r e^{\lambda_r \tau}, \tag{13}$$

in which the entries $h_{g,ij}(\tau)$ and $\dot{h}_{g,ij}(\tau)$ represent, respectively, the displacement and velocity of the ith dof, for $\tau > 0$, caused by a unit impulsive force exerted on the jth dof at $\tau = 0$. Since the application of a unit impulse produces the following set of post-initial conditions

$$\mathbf{h}_g\left(0^+\right) = \mathbf{0} = \sum_{r=1}^{2N_p} \boldsymbol{\psi}_r \boldsymbol{L}_r^{\mathrm{T}}, \tag{14}$$

and

$$\dot{\mathbf{h}}_g\left(0^+\right) = \mathbf{M}_{22}^{-1} = \sum_{r=1}^{2N_p} \lambda_r \boldsymbol{\psi}_r \boldsymbol{L}_r^{\mathrm{T}}, \tag{15}$$

we are allowed to rephrase Eq. (11) as

$$\mathbf{R}(s) = \sum_{r=1}^{2N_p} \left(\frac{\boldsymbol{\psi}_r \boldsymbol{L}_r^{\mathrm{T}} \left(-\lambda_r^2 \mathbf{M}_{21} - \lambda_r \mathbf{C}_{21} - \mathbf{K}_{21}\right)}{s - \lambda_r} \right) + \mathbf{M}_{22}^{-1} \mathbf{M}_{21}. \tag{16}$$

Thus, by defining a novel modal transmission vector

$$\boldsymbol{T}_r = \left(-\lambda_r^2 \mathbf{M}_{21} - \lambda_r \mathbf{C}_{21} - \mathbf{K}_{21}\right)^{\mathrm{T}} \boldsymbol{L}_r, \tag{17}$$

we express the modal partial fraction decomposition of $\mathbf{R}(s)$, evaluated along the frequency axis $s = \mathrm{i}\omega$, as the matrix of R-FRFs

$$\mathbf{R}(\mathrm{i}\omega) = \sum_{r=1}^{2N_p} \left(\frac{\boldsymbol{\psi}_r \boldsymbol{T}_r^{\mathrm{T}}}{\mathrm{i}\omega - \lambda_r} \right) + \mathbf{M}_{22}^{-1} \mathbf{M}_{21}, \tag{18}$$

where the vector $\boldsymbol{T}_r$ provides a combination of mass, stiffness, and damping transmission elements in between the exciting and guided dofs with the modal participation factors $\boldsymbol{L}_r$ of the virtually grounded system. We here name $\mathbf{R}(\mathrm{i}\omega)$ as response-based frequency response matrix. Interestingly, we find a constant term in Eq. (18), related to the mass matrix of the virtually grounded system and to the inertial coupling between guided and driving dofs.

We demonstrate by Eq. (18) that the $\mathbf{R}(\mathrm{i}\omega)$ matrix collects several modal features: poles and mode shapes of the virtually grounded system in addition to the novel modal transmission vector $\boldsymbol{T}_r$. To corroborate the existence of additional local mode shapes in the R-FRFs' matrix, we propose an algebraic identification expounded in Appendix, leading to a polynomial model of $\mathbf{R}(\mathrm{i}\omega)$, closely related to the modal model in Eq. (18). We remark how these additional modal parameters are suitable for carrying out local diagnoses. In fact, they provide an increased sensitivity to local damages with respect to that of modal parameters accessed by the estimation of classical FRFs, which have a global meaning [14,15]. In this respect, Ref. [14] offers an extended discussion carried out on a classical Euler–Bernoulli beam model. In particular, the author investigates the impact of an increasing damage on the lowest three natural frequencies referring to both the real and the virtual system, identified by means of the classical FRFs and R-FRFs matrices, respectively. It is shown how natural frequency changes of virtually grounded systems could be more sensitive than the respective frequency changes of the classical FRFs. In addition, Ref. [15] reports a beam analysis in which undamaged and damaged states are compared by means of modal parameters extracted from both FRFs and R-FRFs matrices. We also emphasize how the possibility of choosing different sets of exciting and free dofs leads to independent evaluations of $\mathbf{R}(\mathrm{i}\omega)$, representing the unconnected virtually achieved boundary conditions. This feature is promising even for the usage of R-FRFs additional modal parameters in the model updating field, as an alternative to that of anti-resonant frequencies [12]. In the next section, we design a specialized identification technique, taking into account the modal decomposition Eq. (18).

3. R-FRFs' identification technique

Several stochastic system identification techniques have been developed to identify the modal parameters of a structure in operating conditions using output-only data [22,23]. These techniques, called as a whole in-operation, operational, or output-only modal analysis (OMA), are based on the assumption that system responses are realizations of stochastic dynamics having unknown white and uncorrelated noises as inputs [24]. In this field, frequency-domain identification methods [25,26] first estimate power spectral densities (PSDs) between N_o responses and certain N_r reference responses, in order to fit them by means of a parametric model. Assuming the operational forces to be white uncorrelated noise sequences, the output PSDs' matrix $\mathbf{S}_{xx}(\mathrm{i}\omega) \in \mathbb{C}^{N_o \times N_r}$ is modally decomposed as follows [27]:

$$\mathbf{S}_{xx}(\mathrm{i}\omega) = \sum_{r=1}^{2N_p} \left(\frac{\boldsymbol{\psi}_r \boldsymbol{K}_r^{\mathrm{T}}}{\mathrm{i}\omega - \lambda_r} + \frac{\boldsymbol{\psi}_r \boldsymbol{K}_r^{\mathrm{T}}}{-\mathrm{i}\omega - \lambda_r} \right), \tag{19}$$

where $\boldsymbol{K}_r$, the so-called operational reference vector, is a combination of the modal parameters and of the unknown input PSD matrix entries. For this reason, the modal participation factors and, by consequence, the modal scale factors cannot be determined from a single OMA test, but appropriate methods for scaling are needed [28–30].

The PSDs' modal decomposition Eq. (19) comprises both positive and negative poles coming from the Fourier transformation of the cross-correlation function matrix $\mathbf{R}_{xx}(\tau)$ [31]. Fourier transforming the sole causal part of $\mathbf{R}_{xx}(\tau)$, with $\tau \geq 0$, leads to the so-called half-spectrum matrix $\mathbf{S}^{+}_{xx}(s)$ [26]. The modal decomposition of this matrix corresponds to the first term in Eq. (19)

$$\mathbf{S}^{+}_{xx}(s) = \sum_{r=1}^{2N_p} \left(\frac{\boldsymbol{\psi}_r \boldsymbol{K}_r^{\mathrm{T}}}{s - \lambda_r} \right). \tag{20}$$

As it is well known, the similar form of modal decompositions Eqs. (5), (19), and (20) allows for the usage of the classical estimation schemes to extract modal parameters from the PSDs' matrix, with the sole different physical meaning of operational reference vectors with respect to modal scale factors. In resembling fashion, by comparing Eqs. (18) and (20), we notice the analogy between the half-spectrum modal model and the R-FRF decomposition, where the modal transmission vectors $\boldsymbol{T}_r$, similarly to the operational reference vectors $\boldsymbol{K}_r$, are a combination of the modal participation factors $\boldsymbol{L}_r$ and physical quantities involved in the transmission of motion between the driving and guided dofs, generally unknown. In order to estimate the modal parameters from R-FRFs, we, thus, may apply identification techniques developed for OMA. We make the choice of using a frequency domain parametric modal method based on the Least Squares Frequency Domain (LSFD) estimator, relying on the modal model in Eq. (18), in combination with the poly-reference Least Squares Complex Frequency (pLSCF) method [28]. The LSFD method is employed to obtain a global estimate of the mode shapes in combination with the pLSCF providing poles and modal transmission vectors.

The adopted pLSCF estimator is based on a Right Matrix Fraction Description (RMFD) in the discrete-time domain of the oth row of the $\mathbf{R}(\mathrm{i}\omega)$ matrix at each radian frequency ω_k as [32]:

$$\mathbf{R}_o(\omega_k) \simeq \mathbf{N}_o(\omega_k, \boldsymbol{\theta}) \mathbf{D}(\omega_k, \boldsymbol{\theta})^{-1}, \tag{21}$$

where for every free dof o ($o = 1, \ldots, m$)

$$\begin{aligned} \mathbf{D}(\omega_k, \boldsymbol{\theta}) &= \sum_{r=0}^{p} \Omega_r(\omega_k) \boldsymbol{\alpha}_r \\ \mathbf{N}_o(\omega_k, \boldsymbol{\theta}) &= \sum_{r=0}^{p} \Omega_r(\omega_k) \boldsymbol{\beta}_{o_r} \end{aligned}, \tag{22}$$

are the denominator $\mathbf{D}(\omega_k, \boldsymbol{\theta}) \in \mathbb{C}^{n \times n}$ and the numerator $\mathbf{N}_o(\omega_k, \boldsymbol{\theta}) \in \mathbb{C}^{1 \times n}$ p-order matrix polynomial containing the unknown matrix real valued coefficients $\boldsymbol{\alpha}_r$ and $\boldsymbol{\beta}_{o_r}$, collected in the matrix $\boldsymbol{\theta}$. The generalized transform variable $\Omega_r(\omega_k)$, named the complex polynomial basis function, is formulated in the z-domain, being equal to $\mathrm{e}^{-\mathrm{i}\omega_k \Delta t}$, where Δt is the sampling period. We introduce the following linear-in-variable error formulation:

$$\boldsymbol{\eta}_o(\omega_k, \boldsymbol{\theta}) = \mathbf{N}_o(\omega_k, \boldsymbol{\theta}) - \mathbf{D}(\omega_k, \boldsymbol{\theta}) \mathbf{R}(\omega_k), \tag{23}$$

in order to obtain a sub-optimal linear least squares problem. This is defined by minimizing the following cost function:

$$l(\boldsymbol{\theta}) = \sum_{o=1}^{N_o} \sum_{k=1}^{N_f} \mathrm{tr}\left[\boldsymbol{\eta}_o^{\mathrm{H}}(\omega_k, \boldsymbol{\theta}) \, \boldsymbol{\eta}_o(\omega_k, \boldsymbol{\theta}) \right], \tag{24}$$

where $\mathrm{tr}[\cdot]$ is the trace of the matrix operator. Once the coefficients of the denominator matrix have been determined, the roots of the denominator polynomial $\mathbf{D}(\omega_k, \boldsymbol{\theta})$ are the eigenvalues of the companion matrix [33]:

$$\mathbf{A}_c = \begin{pmatrix} \mathbf{0} & \mathbf{I} & \cdots & \mathbf{0} \\ \vdots & \vdots & \ddots & \vdots \\ \mathbf{0} & \mathbf{0} & \cdots & \mathbf{I} \\ -\boldsymbol{\alpha}_0 & -\boldsymbol{\alpha}_1 & \cdots & -\boldsymbol{\alpha}_{p-1} \end{pmatrix} \in \mathbb{R}^{pn \times pn}. \tag{25}$$

This eigenvalues, defined in the z-domain, can be converted into the poles Eq. (6), providing the natural frequencies and the damping ratios of the virtually grounded system. The eigenvectors of the companion matrix assume the role of the transmission modal vectors as can be demonstrated by deriving the state-space conversion of the system defined by Eq. (21), adopting the so-called controllable canonical state-space realization [34].

Once the poles and the modal transmission vectors have been computed by means of a stabilization diagram, the virtually grounded system mode shapes can be found, at last, by solving in a linear least squares sense Eq. (18) through the LSFD estimator. In short, to estimate the modal parameters in Eq. (18), we propose a two-step procedure derived from OMA field: (i) a pLSCF estimator allows for achieving virtually grounded system poles and modal transmission vectors by means of a stabilization chart; (ii) a LSFD estimator provides the virtually grounded system mode shapes, whose consistency is expected to be validated by using validation tools as mainly the Modal Assurance Criterion (MAC).

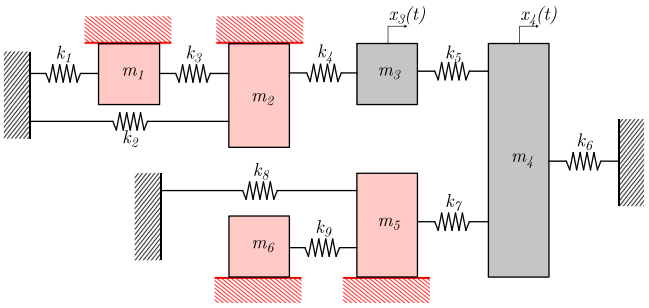

Fig. 1. Schematic of the 6 DOF lumped parameter system virtually grounded on the exciting dofs.

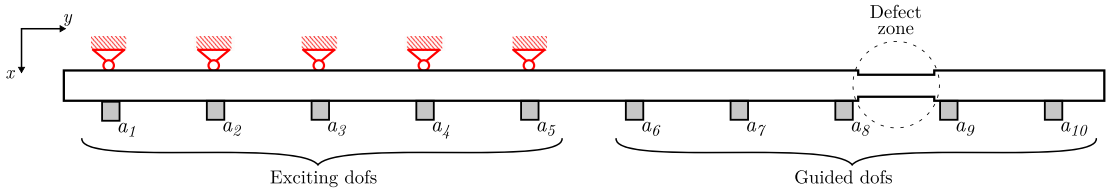

Fig. 2. Schematic of the experimental beam where guided and exciting dofs are highlighted. The virtual supports correspond to the impact locations. The dotted circle between the 8th and 9th accelerometer indicates the damaged zone simulated by a thickness reduction of the beam.

4. Case studies

We perform the modal parameter estimation (MPE), by the procedure described in Section 3, for the following two case studies. Firstly, we analyze the 6-DOF lumped parameter system represented in Fig. 1, considering the hereunder case-based R-FRFs' matrix

$$\begin{pmatrix} Y_3(\mathrm{i}\omega) \\ Y_4(\mathrm{i}\omega) \end{pmatrix}_{1,2,5,6} = \mathbf{R}(\mathrm{i}\omega) \begin{pmatrix} Z_1(\mathrm{i}\omega) \\ Z_2(\mathrm{i}\omega) \\ Z_5(\mathrm{i}\omega) \\ Z_6(\mathrm{i}\omega) \end{pmatrix}_{1,2,5,6}, \tag{26}$$

which relates the guided dofs 3rd and 4th with the exciting 1st, 2nd, 5th and 6th, collected in the loading cases recalled by the notation $(.)_{1,2,5,6}$, featuring the ith mass as subjected to a unit impulse force. Measurement noise is added to all the outputs and inputs to achieve a 50dB signal-to-noise-ratio (SNR) for all signals. After retrieving the matrix $\mathbf{R}(\mathrm{i}\omega)$ by means of the six different estimators proposed in [16], we perform MPE exploiting each of the measured $\mathbf{R}(\mathrm{i}\omega)$. This example is useful to compare the modal parameters, estimated by processing each $\mathbf{R}(\mathrm{i}\omega)$ modal decomposition, with their theoretical values, that is those of the system for which the excited masses are virtually grounded, as shown in Fig. 1.

Secondly, we examine the outcome of experiments performed on a slender PMMA beam, in a healthy and damaged state. Specifically, the specimen is a beam of length, width, and thickness equal to 1000 mm, 60 mm, and 35 mm, respectively; material properties and resonance frequencies of the completely free PMMA beam are characterized and determined in [15]. Damage is obtained by locally reducing the beam thickness of 3.5 mm per side, from 35 mm to 28 mm: the position of the artificial damage is sketched in the highlighted area of Fig. 2. In this case, the case-based R-FRFs matrix is

$$\begin{pmatrix} \ddot{Y}_6(\mathrm{i}\omega) \\ \ddot{Y}_7(\mathrm{i}\omega) \\ \ddot{Y}_8(\mathrm{i}\omega) \\ \ddot{Y}_9(\mathrm{i}\omega) \\ \ddot{Y}_{10}(\mathrm{i}\omega) \end{pmatrix}_{1,2,3,4,5} = \mathbf{R}(\mathrm{i}\omega) \begin{pmatrix} \ddot{Z}_1(\mathrm{i}\omega) \\ \ddot{Z}_2(\mathrm{i}\omega) \\ \ddot{Z}_3(\mathrm{i}\omega) \\ \ddot{Z}_4(\mathrm{i}\omega) \\ \ddot{Z}_5(\mathrm{i}\omega) \end{pmatrix}_{1,2,3,4,5} \tag{27}$$

that ensures to virtually support the left undamaged part of the beam at a_{1-5} locations, where the impacts occur, as sketched in Fig. 2. We, thus, compare the modal parameters extracted from several $\mathbf{R}(\mathrm{i}\omega)$ measurements in the two beam states, showing the local meaning of the R-FRFs, in addition to the good sensitivity of the R-FRFs modal parameters in the case of the damaged beam. We clarify this point by performing a further analysis, based on nine different $\mathbf{R}(\mathrm{i}\omega)$ definitions, focusing on several local portions of the beam, aimed at elucidating the performance of the technique for localizing the damage. The same analysis is repeated for several damage configurations simulated on a finite element (FE) beam model inspired by the sample used in the experimental case.

The aforementioned six different estimators, introduced in Ref. [16] and used in the following analyses, are, specifically, $\mathbf{R}_1$ and $\mathbf{R}_v$ defined by means of a reformulation of the classical H_1 and H_v estimators for FRFs, while $\mathbf{R}_{\mathrm{ar}}$, $\mathbf{R}_{\mathrm{EV}}$, and $\mathbf{R}_{\log}$ come from

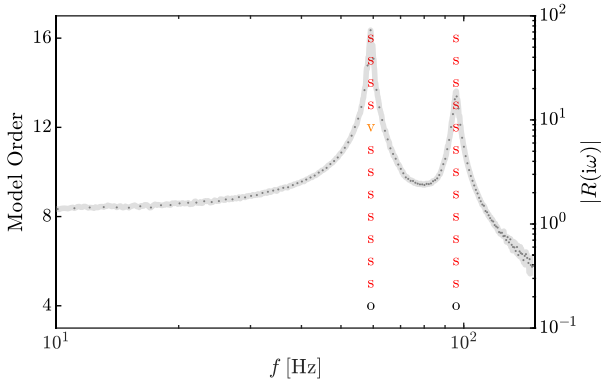

Fig. 3. Identification of the lumped parameter system by using R_v estimated R-FRFs: stabilization diagram along with the magnitude of the R-FRFs sum function, blue line. Each stable pole is indicated with an 's' and the model order is reported on the left y-axis.

Table 1
Identification of the lumped parameter system using R_v estimated R-FRFs: comparison between exact and estimated modal parameters.

	Natural frequency (Hz)			Damping ratio (%)		
	Exact	Estimated	$\lvert\Delta\rvert$ (%)	Exact	Estimated	$\lvert\Delta\rvert$ (%)
Mode 1	59.17	59.19	0.0408	0.929	0.8797	5.340
Mode 2	95.73	95.78	0.0530	1.504	1.365	9.223

a re-conceptualization of the nonparametric FRF estimators proposed in [35]. Importantly, the sole input–output estimator $\mathbf{R}_{\text{def}}$ results available only if input signals are measured and included in its computation. Actually, the definition of this latter estimator is obtained by relying on the relationship $\mathbf{R}(i\omega) = \mathbf{H}_{21}(i\omega)\mathbf{H}_{11}^{-1}(i\omega)$, where $\mathbf{H}_{11}$ and $\mathbf{H}_{21}$ indicate the corresponding partitions of the FRF matrix $\mathbf{H}(i\omega) = \mathbf{B}^{-1}(i\omega)$ (see Eq. (2)).

4.1. Identification of the lumped parameter system

We, here, show the results of the identification procedure in the case of the $\mathbf{R}_v$ estimation of the R-FRFs matrix. From the pLSCF, we build up the stabilization diagram reported in Fig. 3, subsequently assuming an increasing number of the model order p of Eq. (21). The stabilization diagram gives a strong indication of the two physical modes, allowing for the selection of the corresponding stable poles, indicated with the letter 's'. The pair of natural frequencies and damping ratios, computed from the two selected stable poles, are reported in Table 1 in addition to the exact modal parameters of the system when considered grounded in the exciting dofs. The relative percentage error $\Delta = 100 \times (v_{\text{th}} - v_{\text{est}})/v_{\text{th}}$ between theoretical and estimated values is also provided for both natural frequencies and damping ratios, here denoted by the generic symbol v.

Once poles and modal transmission vectors are computed by the first step of the procedure, we complete the MPE by deploying the LSFD estimator, to compute the unscaled mode shapes. Afterwards, we compare the data synthesized from the modal model of Eq. (18) with the measured data as shown in Fig. 4. The visual match, together with a high correlation coefficient for all the R-FRFs, proves the goodness of the MPE process results.

We repeat the identification process, starting from each of the six different $\mathbf{R}(i\omega)$ estimates [16]. In Table 2, we summarize the computed natural frequencies and damping ratios, together with the relative percentage error obtained with respect to the exact values in Table 1. Fig. 5 shows the said discrepancies of Table 2 in a graphical fashion.

The identification results show a very good agreement between the theoretical poles of the virtually grounded system (Fig. 1) and those extracted from the $\mathbf{R}(i\omega)$ matrix by means of the pLSCF estimator. Negligible errors are observed for the identified natural frequencies, while higher errors characterize the estimated damping ratios. The MPE performed by $\mathbf{R}_{\text{EV}}$, $\mathbf{R}_v$, and $\mathbf{R}_{\text{def}}$ estimates leads to better results in terms of damping ratios, showing errors less than 10% for both system modes. We highlight the total agreement between the modal parameter accuracy and the performance of the different R-FRFs' estimators, as pointed out in Fig. 5. The proposed comparison is a further check of the R-FRFs' modal model formulation, derived in Section 3, and of its strong analogy with the modal expression of the half-spectrum matrix.

4.2. Identification of the PMMA beam

In the experimental case study, we perform the identification process considering a slender PMMA beam in two states: a healthy reference state and a damaged one, obtained by introducing a thickness reduction as depicted in Fig. 2. We process the specialized $\mathbf{R}(i\omega)$ matrix of Eq. (27), which relates the guided x-accelerations from the sensor a_6 to a_{10} with the exciting ones from a_1 to a_5.

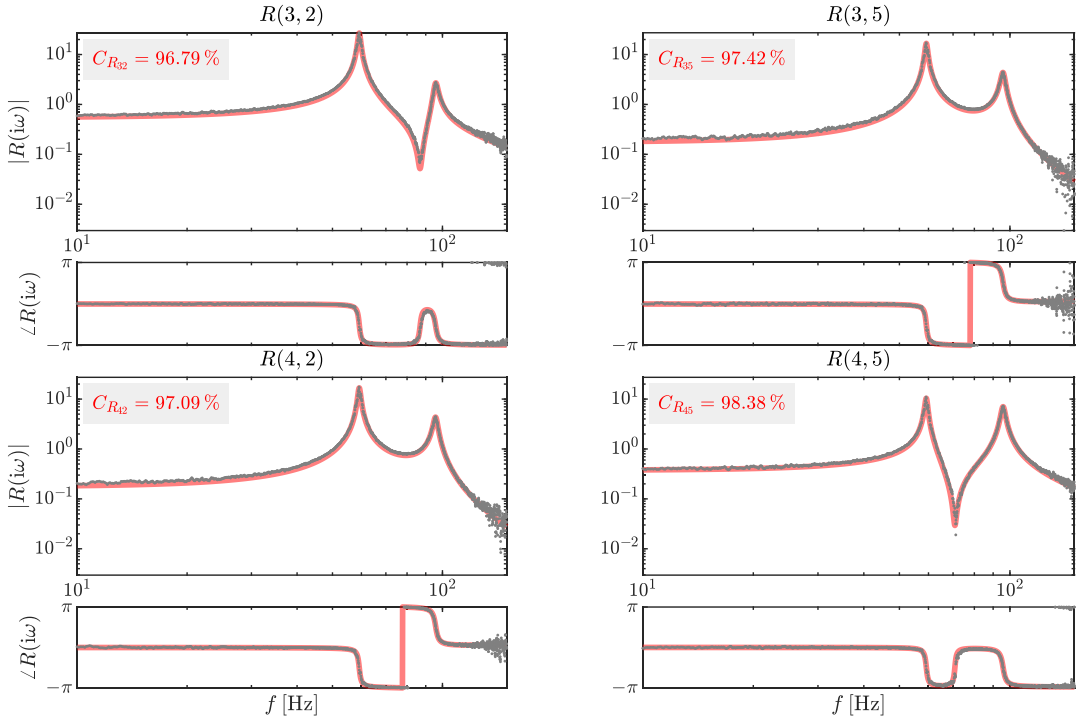

Fig. 4. R-FRFs in the case of the lumped parameter system: comparison between R_v estimated R-FRFs, dotted lines, and syntheses by modal model, solid lines.

Table 2
Identification of the lumped parameter system: comparison between exact and estimated modal parameters computed by using the different R-FRFs estimators [16].

		Natural frequency (Hz)		Damping ratio (%)	
		Estimated	$\lvert\Delta\rvert$ (%)	Estimated	$\lvert\Delta\rvert$ (%)
R_{ar}	Mode 1	59.15	0.0243	0.7636	17.84
	Mode 2	95.77	0.0355	1.342	10.78
R_{EV}	Mode 1	59.19	0.0367	0.8726	6.110
	Mode 2	95.78	0.0524	1.366	9.174
R_{log}	Mode 1	59.11	0.0966	0.9924	6.782
	Mode 2	95.89	0.1737	1.192	20.71
R_1	Mode 1	59.21	0.0735	1.263	35.89
	Mode 2	95.79	0.0620	1.460	2.916
R_v	Mode 1	59.19	0.0408	0.8797	5.340
	Mode 2	95.78	0.0530	1.365	9.223
R_{def}	Mode 1	59.19	0.0331	0.8727	6.095
	Mode 2	95.78	0.0532	1.365	9.249

Figs. 6 and 7 show the $\mathbf{R}_{def}$ estimate of these particular R-FRFs in terms of magnitude and phase angle. We notice the existence of sliding effects on all the R-FRFs, due to the damage occurrence on the beam side, included in the free dofs. This frequency shifting is more evident for the second and third peak, owing to the lower measurement accuracy in the low-frequency range. The virtually constrained system defined by the specialized $\mathbf{R}(\mathrm{i}\omega)$ matrix is schematized in Fig. 2, where virtual supports are introduced on the left undamaged part of the beam, in correspondence to the y-coordinates of the impact load locations.

We, here, show the MPE procedure performed using the $\mathbf{R}_{def}$ measurements of the beam in the healthy and damaged states. In this regard, we process the last column of the $\mathbf{R}(\mathrm{i}\omega)$ matrix that ensures the estimation of the only 5th component of the modal transmission vector $\boldsymbol{T}_r$ for each mode, see Eq. (18). Such a component provides an higher "participation" of the three modes in the frequency range, which means an higher value of peak amplitudes as shown in Fig. 6, because of the coupling between the 5th sensor, representing one of the driving dofs, and the guided sensors from a_6 to a_{10}. In such an interpretation, the detection of virtual system modes and the extent of their contribution to the response are related to modal transmission vectors, which are the counterpart of modal participation vectors in the classical FRFs, as comparing Eqs. (5) to (18) implies. By the pLSCF estimator, we build up the stabilization diagrams in Fig. 8. The stabilization diagrams give a strong indication of the three physical modes,

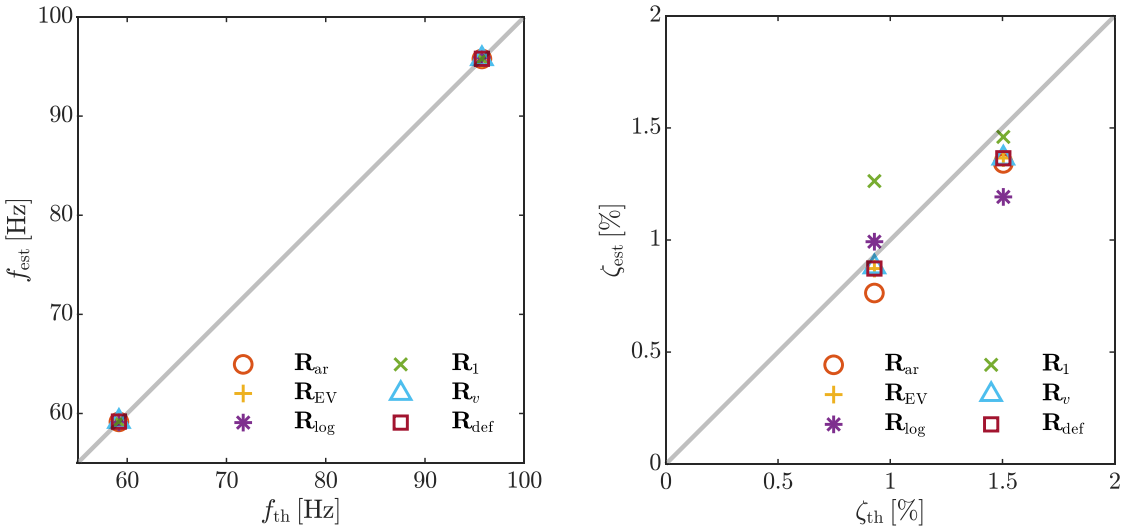

Fig. 5. Representation of estimated modal parameters' deviations from corresponding theoretical values, in the case of the lumped parameter system, as collected in Table 2.

allowing for the selection of the corresponding stable poles. The stability of the first candidate mode is affected by the poor quality of the first peak, as visible especially in the damaged beam state. Natural frequencies and damping ratios computed from the selected poles are reported in Table 3.

In the second identification step, we retrieve the estimates of the mode shape vectors by means of the LSFD estimator. In Fig. 9, the three unscaled mode shapes, real part, are reported for the two beam states.

The m components of each modal vector $\boldsymbol{\psi}_r$ correspond to the guided dofs of the beam, whose locations are those of the five accelerometers from a_6 to a_{10}. The corresponding autoMAC values are reported for each set of modes, showing their orthogonality. As demonstrated in Section 3 and reported in [14], for the case of a finite-element beam model, the mode shapes extracted by matrix $\mathbf{R}(\mathrm{i}\omega)$ comprise those of the original beam considered virtually constrained at the exciting dofs' locations. The correct virtual boundary conditions depend on the considered signals; in the present case, the y-accelerations from sensors a_1 to a_5 play the role of the grounded dofs with boundary conditions $u_1^{(v)}(t) = \cdots = u_5^{(v)}(t) = 0$, where $u(t)$ is the beam's deflection along the x-axis direction, t is the time variable, and the superscript $(.)^{(v)}$ recalls that the deflection is related to the virtually grounded system.

As for the previous case study, we repeat the identification process by using each of the six different $\mathbf{R}(\mathrm{i}\omega)$ estimates regarding the two beam's states. The relative percentage variation $\Delta = 100 \times (v_{\text{h}} - v_{\text{d}})/v_{\text{h}}$, between the healthy and damaged state quantities is also computed for both frequencies and damping ratios, here denoted by the generic symbol v.

The MPE procedure leads to the identification of all the three modes only in the case of $\mathbf{R}_{\text{ar}}$ and $\mathbf{R}_{\text{def}}$ processing, while the other estimators show lower accuracy in the low-frequency range, severely affecting the stability of the first pole. The 2nd and 3rd resonance frequencies undergo a significant negative shift, of around 10%, which, as reported in [15], is almost double compared to the frequency variations of those of the original beam. The 1st mode, when available, exhibits an opposite frequency shift. Looking at the damping ratios in Table 3, we find to inspect significant symptoms more difficult owing to the higher uncertainty of the estimates. We comment that, generally, the 2nd mode damping ratio decreases, except for the results from $\mathbf{R}_1$ processing, while the 3rd one increases. Here, we find important to better elucidate the local meaning of the additional poles and modes that compose $\mathbf{R}(\mathrm{i}\omega)$ matrix. By suitably changing the exciting dofs, together with the loading conditions, we are allowed to perform different analyses, based on several $\mathbf{R}(\mathrm{i}\omega)$ matrices, each containing modal parameters of a specialized virtual subsystem. These additional modal parameters exhibit a different sensitivity with respect to the damage location, allowing SHM to be performed with a local approach. In the beam case, we, specifically, collect ten different loading conditions, each defined by the presence of an impulsive load on the ith accelerometer position along the x-direction. We, thus, easily change the two response subsets' definition, the exciting and the free dofs' subsets, making possible the statement of several versions of the matrix relationship Eq. (3). We classify two accelerometers as guided dofs, and the remaining eight as exciting dofs, in order to inspect different free beam portions. Changing the pair of sensors classified as free, we perform nine analyses, following the identification procedure described in Section 3. We compute the first natural frequency of each of the nine virtually grounded systems, both in the healthy and damaged state. The percentage relative variation $\Delta(\%)$ is used to compare this modal parameter in the two beam states. In Table 4 and Fig. 10, we collect the results derived by the MPE process on the nine $\mathbf{R}(\mathrm{i}\omega)$ measurements.

We notice how the damage occurrence, located in between the 8th and 9th accelerometer locations, becomes affecting more significantly the first natural frequency of the virtual system, as its unconstrained dofs get closer to the damage itself. Specifically, the 8th and 9th cases, that focus on a beam portion that includes the reduced beam sections, exhibit a frequency shift $\Delta(\%)$ remarkably greater than those of the other cases. In this sense, the local meaning of the additional modes, which compose the R-FRFs, indirectly conveys the novel idea of developing indicators and designated strategies for local structural diagnoses.

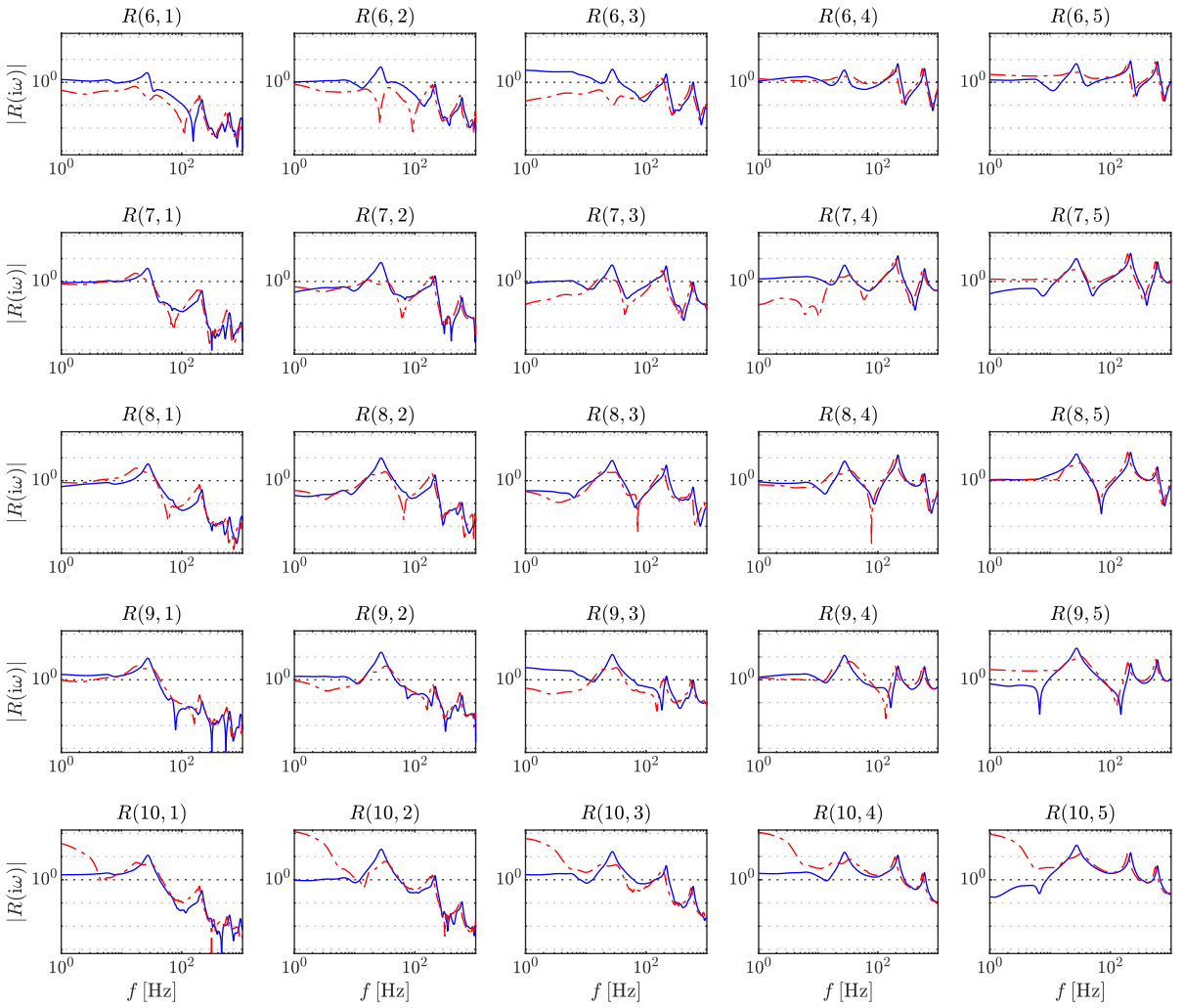

Fig. 6. Magnitude of R-FRFs, computed by using R_{def} estimator, in the case of the PMMA beam: healthy state, blue solid line, damaged state, red dashed line. (For interpretation of the references to color in this figure legend, the reader is referred to the web version of this article.)

4.3. Identification in presence of multiple damages

Here, we extend the analysis proposed in Table 4 and Fig. 10, to the case of multiple damages affecting the beam structure. Firstly, we reproduce the result of Fig. 10, through a FE simulation of the beam previously experimentally tested. By the FE modeling approach, we are allowed for exploring different damage configurations which would turn out to be time consuming if carried out by an experimental campaign. Second, we focus on specific cases, each characterized by the location of an additional damage and its extent. We, thus, model the presence of a second damage, still modeled as a local reduction in beam thickness, with the aim of investigating the following three configurations: (i) additional equal damage, having a similar reduction in beam thickness, from 35 mm to 28 mm, positioned between the 2nd and 3rd accelerometer locations; (ii) additional equal damage between the 5th and 6th accelerometer locations; (iii) additional more severe damage, having a double beam thickness reduction, from 35 mm to 21 mm, placed between the 2nd and 3rd accelerometer locations. Changing the pair of free sensors as schematized in Table 4, we perform nine analyses, following the identification procedure described in Section 3. We, then, compute the first natural frequency of each of the nine virtually grounded systems, in the new damaged states. The variation of such a natural frequency, with respect to the healthy beam state, is reported in the following Fig. 11.

By using the single damage case as reference (green curve with diamond markers in Fig. 11), we notice that the occurrence of an additional symmetric damage of equal importance (red curve with square markers in Fig. 11) affects the natural frequencies of virtual subsystems including the second damage, in a similar way, as expected. This variation becomes more evident on the side where the added damage is more severe, as shown by the yellow curve with triangle markers in Fig. 11. In the case of an additional centered damage (blue curve with circle markers), the frequency decrease is magnified for the majority of the subsystems having

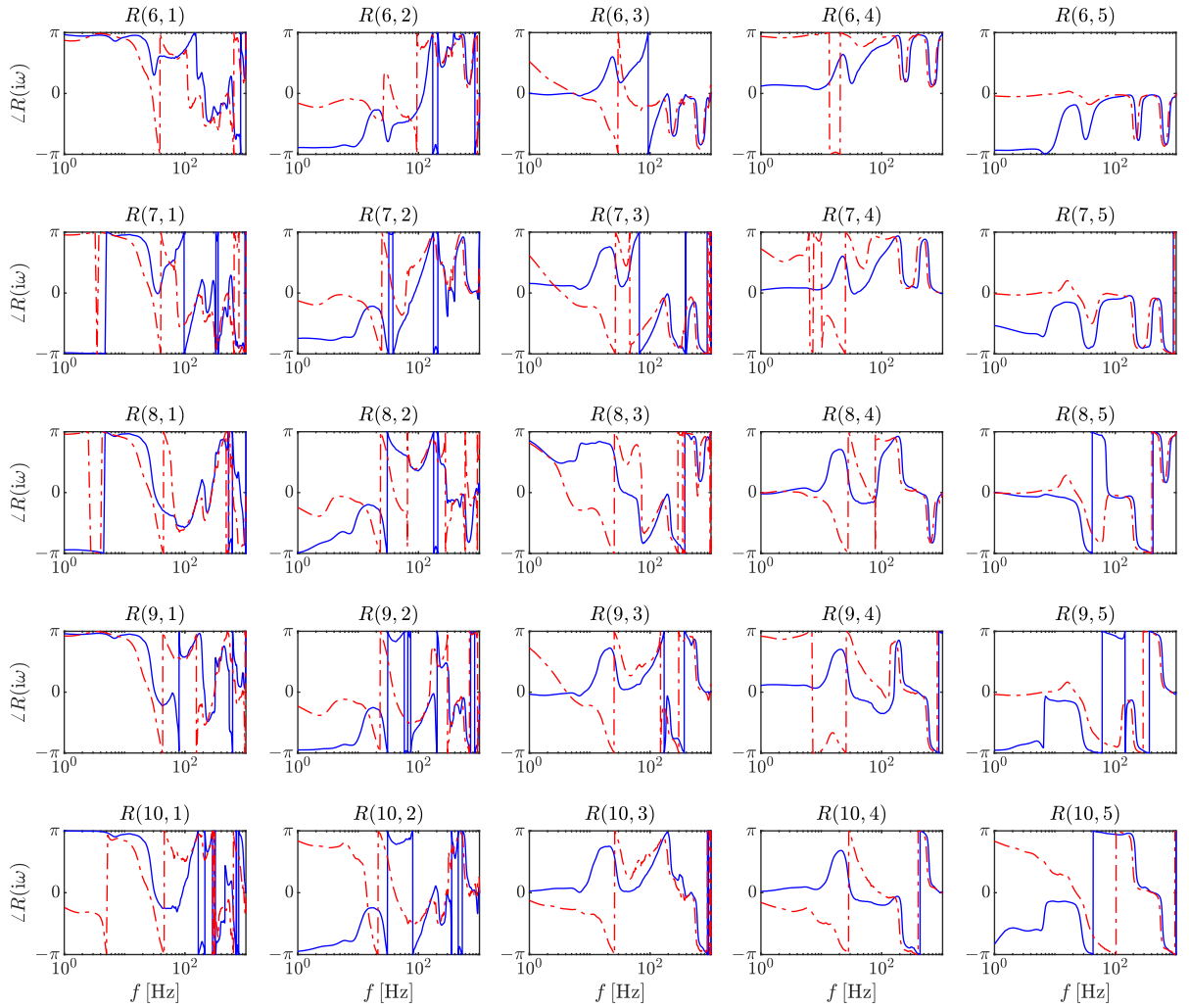

Fig. 7. Phase of R-FRFs, computed by using R_{def} estimator, in the case of the PMMA beam: healthy state, blue solid line, damaged state, red dashed line. (For interpretation of the references to color in this figure legend, the reader is referred to the web version of this article.)

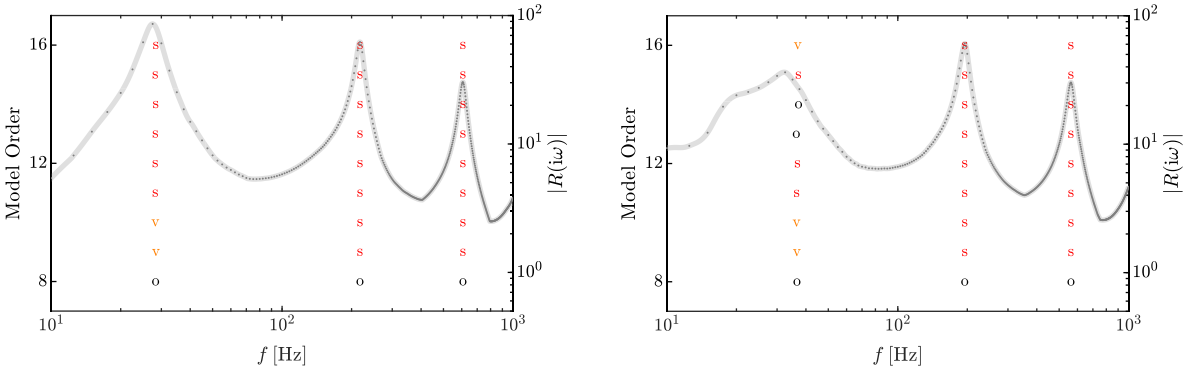

(a) Healthy: stabilization diagram

(b) Damaged: stabilization diagram

Fig. 8. Identification of the healthy (a) and damaged (b) PMMA beam by using R_{def} estimated R-FRFs: stabilization diagram along with the magnitude of the R-FRFs sum function, dotted line.

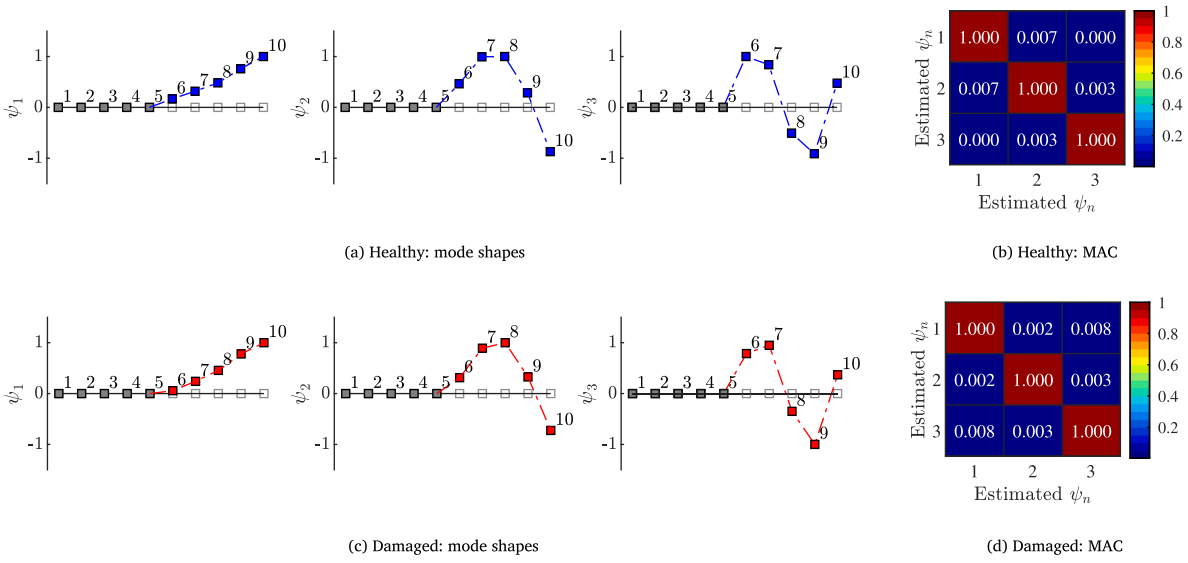

(a) Healthy: mode shapes

(b) Healthy: MAC

(c) Damaged: mode shapes

(d) Damaged: MAC

Fig. 9. Identification of the healthy (a)–(b) and damaged (c)–(d) PMMA beam by using R_{def} estimated R-FRFs: (a)–(c) estimated modal vectors, (b)–(d) autoMAC from the estimated modal vectors' set.

Table 3
Identification of the PMMA beam: comparison between the estimated modal parameters, in the cases of the healthy and the damaged state, computed by using the different R-FRFs' estimators [16].

		Natural frequency (Hz)			Damping ratio (%)		
		Healthy	Damaged	Δ (%)	Healthy	Damaged	Δ (%)
R_{ar}	Mode 1	28.98	33.65	16.132	14.69	8.195	−44.23
	Mode 2	218	196.9	−9.649	3.776	3.739	−0.976
	Mode 3	608	563.2	−7.378	2.995	3.217	7.401
R_{EV}	Mode 1		33.90			3.789	
	Mode 2	217.3	195.2	−10.159	4.674	3.725	−20.30
	Mode 3	606.9	564.1	−7.055	2.802	2.942	5.013
R_{log}	Mode 1						
	Mode 2	218.3	196.4	−9.996	3.179	3.166	−0.399
	Mode 3	607.9	563.6	−7.296	2.981	3.354	12.486
R_{1}	Mode 1						
	Mode 2	216.9	194.7	−10.24	4.532	4.800	5.903
	Mode 3	607.3	562.2	−7.422	3.160	3.3127	4.826
R_{v}	Mode 1						
	Mode 2	218.4	197.5	−9.555	3.139	3.087	−1.664
	Mode 3	607.5	562.6	−7.391	3.017	3.291	9.113
R_{def}	Mode 1	28.11	36.55	30.02	4.265	12.10	183.8
	Mode 2	217.6	194.9	−10.40	3.172	3.168	−0.141
	Mode 3	607.4	562.6	−7.373	3.003	3.207	6.795

the free dofs belonging to the corresponding half of the beam. In this sense, the additional modes, composing the R-FRFs, preserve a keen ability to locate multiple damages and predict their extent. These features could be exploited in the context of optimizing the sensors' layout and/or the set of virtual boundary conditions, more related to the number of sensors and their locations, in order to improve the identification accuracy of multiple damage types and distributions.

5. Conclusions

In this paper, we further analyzed the significance and the role of a specific class of global TFs, here referred to as R-FRFs, in the areas of identification and monitoring of structures. In order to extend the usage of the MPE methods, employed in EMA and OMA, to global transmissibilities, we developed an innovative modal partial fraction decomposition of the R-FRFs, containing additional poles and mode shapes of the original system, when considered virtually constrained to ground at the exciting dofs locations. Specifically, those new, virtual boundary conditions depend on the signals classified as exciting dofs and, moreover, the virtually constrained to ground system responses are observed in correspondence of the free dofs. In addition to poles and modes of

Table 4
Local diagnoses of the PMMA beam: comparison between the estimated first natural frequency, in the cases of the healthy and the damaged state, extracted from the collection of R-FRFs obtained by changing the definition of guided and exciting dofs.

Guided dofs	Exciting dofs	Natural frequency (Hz)		
		Healthy	Damaged	$\lvert\Delta\rvert$ (%)
1, 2	3, 4, 5, 6, 7, 8, 9, 10	145.0	141.1	−2.666
2, 3	1, 4, 5, 6, 7, 8, 9, 10	458.2	451.2	−1.526
3, 4	1, 2, 5, 6, 7, 8, 9, 10	594.9	588.6	−1.067
4, 5	1, 2, 3, 6, 7, 8, 9, 10	604.6	605.3	0.1266
5, 6	1, 2, 3, 4, 7, 8, 9, 10	613.3	604.3	−1.463
6, 7	1, 2, 3, 4, 5, 8, 9, 10	606.8	582.4	−4.016
7, 8	1, 2, 3, 4, 5, 6, 9, 10	604.5	593.0	−1.894
8, 9	1, 2, 3, 4, 5, 6, 7, 10	465.9	432.5	−7.163
9, 10	1, 2, 3, 4, 5, 6, 7, 8	147.8	120.6	−18.42

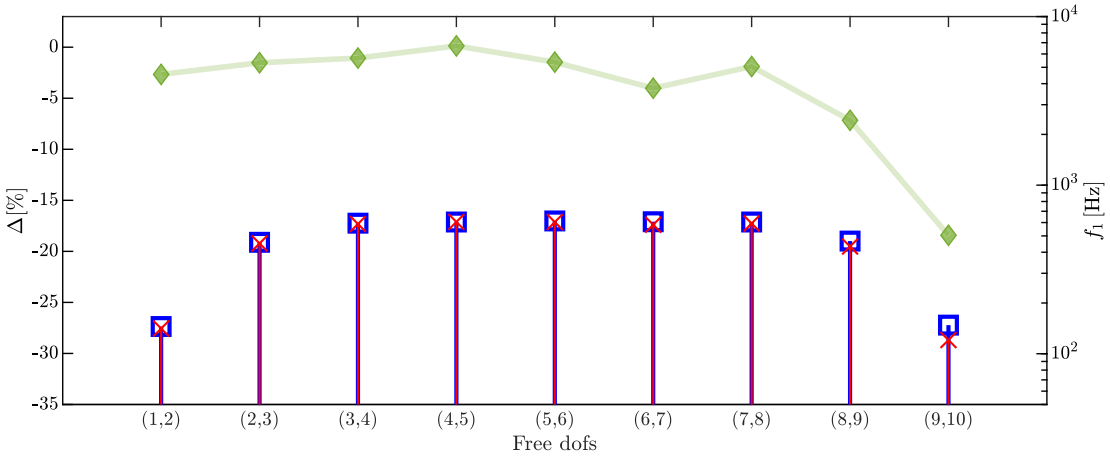

Fig. 10. Local diagnoses of the PMMA beam: comparison between the estimated first natural frequency, in the cases of the healthy, blue square, and damaged state, red cross. The green stems indicate the relative percentage frequency variation. The frequency value is indicated on the right y-axis and the percentage relative shift on the left one. (For interpretation of the references to color in this figure legend, the reader is referred to the web version of this article.)

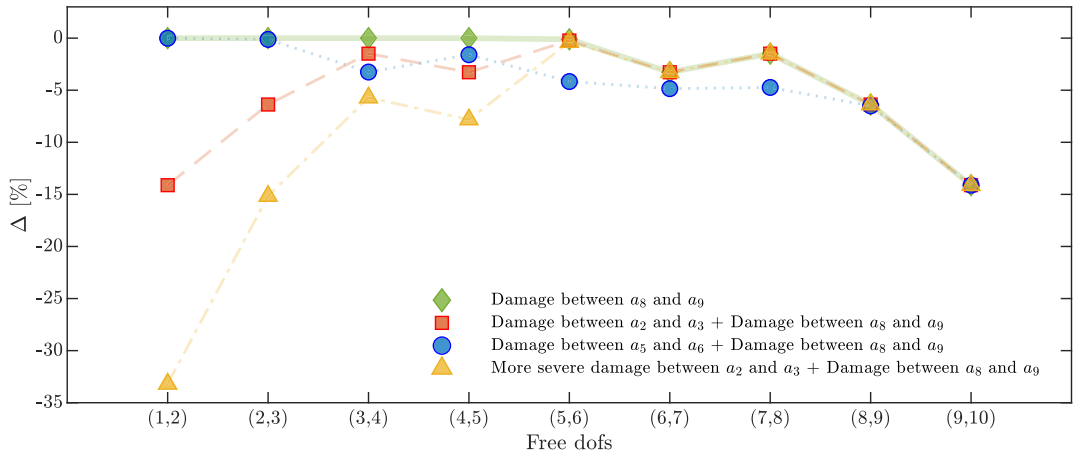

Fig. 11. Local diagnoses of the PMMA beam FE model: comparison between the relative percentage variation of the first resonance frequency, in the cases of the healthy and the different proposed damaged states. (For interpretation of the references to color in this figure legend, the reader is referred to the web version of this article.)

the virtual subsystem, the proposed modal model of the R-FRFs involves novel modal transmission vectors, which derive from the combination of some physical lumped parameters, related to the transmission elements existing between the exciting and the free dofs, and the modal participation factors of the virtually constrained system. We highlighted the strong analogy between the R-FRFs

modal model and that of the half-spectrum matrix, which allowed us to perform MPE, by making usage of the pLSCF algorithm combined with the LSFD method, both typically employed, in tandem, in the OMA field. By presenting different numerical and experimental case studies, we underlined the fundamental aspect of the local meaning of the estimated modal parameters. Actually, by suitably changing the exciting dofs' locations, to make different analyses based on independent R-FRFs becomes possible, each containing modal features of a particular virtual subsystem. This key point has been elucidated and corroborated by performing local diagnoses on an experimental PMMA beam aimed at inspecting the sensitivity of the additional poles estimated from R-FRFs with respect to damage location. Furthermore, the corresponding additional modes are effectively usable in SHM, relying on their higher sensitivity to local changes with respect to that of the classical modes. This magnification of a structural change results from processing the R-FRFs related to different virtually constrained sub-structures, all including the damage to be detected. Further developments of this work will focus on relaxing the definition and the number of usable exciting dofs' locations and on including the usage of the modal transmission vectors, with the aim of scaling the mode shapes. In addition, the here proposed approach, based on local diagnosis, may be extended to the analysis of more complex structures such as plates or frame structures that could better elucidate the R-FRFs' abilities. Lastly, including acoustic pressure responses in this framework represents a potential future development.

CRediT authorship contribution statement

Simone De Carolis: Conceptualization, Methodology, Software, Validation, Formal analysis, Investigation, Resources, Data curation, Writing – original draft, Writing – review & editing, Visualization, Supervision. **Arcangelo Messina:** Conceptualization, Methodology, Software, Validation, Formal analysis, Investigation, Resources, Data curation, Writing – original draft, Writing – review & editing, Visualization, Supervision. **Leonardo Soria:** Conceptualization, Methodology, Software, Validation, Formal analysis, Investigation, Resources, Data curation, Writing – original draft, Writing – review & editing, Visualization, Supervision.

Data availability

Data will be made available on request.

Appendix. Algebraic identification of additional local mode shapes associated to additional local poles in R-FRFs' matrix

Moving from the set of motion equations related to the m free dofs, we write

$$\mathbf{B}_{21}(s)\,\mathbf{Z}(s)+\mathbf{B}_{22}(s)\,\mathbf{Y}(s)=\mathbf{0}, \tag{A.1}$$

which implies the linear output–output relationship of Eq. (3), where matrix $\mathbf{R}(s)$ is

$$\mathbf{R}(s)=-\frac{\operatorname{adj}\left(\mathbf{B}_{22}(s)\right)}{\left|\mathbf{B}_{22}(s)\right|}\mathbf{B}_{21}(s). \tag{A.2}$$

We notice that the poles λ_r of the $\mathbf{R}(s)$ matrix are related to characteristic polynomial of $\mathbf{B}_{22}(s)$, indicated by $|\mathbf{B}_{22}(s)|$, which is a real coefficient polynomial of degree $2m$. These are the poles of the virtually grounded system, obtained from the original system Eq. (2) when subjected to the $\mathbf{Z}(s)=\mathbf{0}$ boundary conditions.

In order to find the mode shape vector for each λ_r, we can use the following set of equations

$$\mathbf{B}_{22}\left(\lambda_r\right)\mathbf{Y}_r=\mathbf{0}, \tag{A.3}$$

where $\mathbf{Y}_r=\boldsymbol{\psi}_r\in\mathbb{C}^{m\times 1}$ is the rth eigenvector of the system represented by the transfer matrix $\mathbf{H}_g(s)=\mathbf{B}_{22}^{-1}(s)$. The main idea is to retrieve these additional modal parameters, belonging to the virtually grounded system $\mathbf{H}_g(s)$, from matrix $\mathbf{R}(s)$ which is strongly related to $\mathbf{B}_{22}$ as expressed in Eq. (A.2). By inspecting the $\mathbf{R}(s)$ matrix entries from a polynomial point of view, we may state

$$R_{ij}(s)=\frac{\sum_{q=0}^{2(m-1)}\beta_{ij,q}^{22}s^q}{\sum_{p=0}^{2m}\alpha_p s^p}\sum_{r=0}^{2}\beta_{ij,r}^{21}s^r, \tag{A.4}$$

where $\beta_{ij,q}^{22}\in\mathbb{R}$ are the real-valued polynomial coefficients of matrix $\operatorname{adj}\left(\mathbf{B}_{22}(s)\right)$ entries, $\alpha_p\in\mathbb{R}$ those of the characteristic equation, and $\beta_{ij,r}^{21}\in\mathbb{R}$ refer to $\mathbf{B}_{21}(s)$ entries that can be easily expressed as

$$-B_{ij}^{21}(s)=\sum_{v=0}^{2}\beta_{ij,v}^{21}s^v=-m_{ij}^{21}s^2-c_{ij}^{21}s-k_{ij}^{21}, \tag{A.5}$$

where m_{ij}^{21}, c_{ij}^{21}, k_{ij}^{21}, respectively, indicate the ij-entries of the matrices $\mathbf{M}^{21}$, $\mathbf{C}^{21}$, $\mathbf{K}^{21}$. By multiplying the two numerator polynomials in Eq. (A.4), we may generally express

$$R_{ij}(s)=\frac{\sum_{k=0}^{2m}\beta_{ij,k}s^k}{\sum_{p=0}^{2m}\alpha_p s^p}, \tag{A.6}$$

where $\beta_{ij,k} \in \mathbb{R}$ are a combination of $\beta^{22}_{ij,q}$ and $\beta^{21}_{ij,r}$. By using the partial fractions expansion in the case where the numerator degree is equal to that of the denominator, we rephrase $R_{ij}(s)$ as

$$R_{ij}(s) = a^{(0)}_{ij} + \sum_{k=1}^{2m} \frac{a^{(k)}_{ij}}{s - \lambda_k}, \tag{A.7}$$

where a^{k}_{ij} are complex-valued coefficients and a^{0}_{ij} is a constant term related to certain entries in the mass matrix that represents the coefficient of the highest term and embodies the remainder of the polynomial division. By using the matrix notation

$$\mathbf{R}(s) = \begin{bmatrix} a^{(0)}_{11} & \cdots & a^{(0)}_{n1} \\ \vdots & \ddots & \vdots \\ a^{(0)}_{m1} & \cdots & a^{(0)}_{mn} \end{bmatrix} + \sum_{k=1}^{2m} \begin{bmatrix} \frac{a^{(r)}_{11}}{s - \lambda_k} & \cdots & \frac{a^{(k)}_{1n}}{s - \lambda_k} \\ \vdots & \ddots & \vdots \\ \frac{a^{(k)}_{m1}}{s - \lambda_k} & \cdots & \frac{a^{(k)}_{mn}}{s - \lambda_k} \end{bmatrix} = \mathbf{A}^{(0)} + \sum_{k=1}^{2m} \frac{\mathbf{A}^{(k)}}{s - \lambda_k}, \tag{A.8}$$

where $\mathbf{A}^{(k)} \in \mathbb{C}^{m \times n}$ are the so-called residual matrices and $\mathbf{A}^{(0)}$ is a constant term. Pre-multiplying both sides of Eq. (A.8) by the factor $(s - \lambda_r)\mathbf{B}_{22}(s)$, referring to a generic rth pole, we obtain

$$\left(s - \lambda_r\right) \mathbf{B}_{22}(s)\, \mathbf{R}(s) = \left(s - \lambda_r\right) \mathbf{B}_{22}(s)\, \mathbf{A}^{(0)} + \sum_{k=1,\, k \neq r}^{2m} \frac{\left(s - \lambda_r\right) \mathbf{B}_{22}(s)\, \mathbf{A}^{(k)}}{s - \lambda_k} + \mathbf{B}_{22}(s)\mathbf{A}^{(r)}, \tag{A.9}$$

and by taking the limit of both sides as s approaches λ_r

$$\lim_{s \to \lambda_r} \left(s - \lambda_r\right) \mathbf{B}_{22}(s)\, \mathbf{R}(s) = \mathbf{0} = \mathbf{B}_{22}\left(\lambda_r\right) \mathbf{A}^{(r)}, \tag{A.10}$$

we notice that, similarly to the definition in Eq. (A.3), each column of $\mathbf{A}^{(r)}$ is proportional to the rth eigenvector of the virtually grounded system $\mathbf{H}_g(s)$.

By the above considerations, we, thus, prove the existence of mode shapes, belonging to the virtually grounded system, in the algebraic structure of the R-FRFs matrix. Actually, as derived in Section 2, we are allowed to express the generic rth residue matrix from the modal model Eq. (18), equivalent to the polynomial representation Eq. (A.8) as

$$\boldsymbol{\psi}_r \boldsymbol{T}_r^{\mathrm{T}} = \begin{bmatrix} \phi_{1,r} T_{1,r} & \cdots & \phi_{1,r} T_{n,r} \\ \vdots & \ddots & \vdots \\ \phi_{m,r} T_{1,r} & \cdots & \phi_{m,r} T_{n,r} \end{bmatrix} = \mathbf{A}^{(r)}, \tag{A.11}$$

where, specifically, the components of the modal transmission vector could be expounded as

$$\boldsymbol{T}_r = \left(-\lambda_r^2 \mathbf{M}_{21} - \lambda_r \mathbf{C}_{21} - \mathbf{K}_{21}\right)^{\mathrm{T}} \boldsymbol{L}_r = \begin{Bmatrix} \sum_{k=1}^{m} \left(-\lambda_r^2 m^{21}_{k1} - \lambda_r c^{21}_{k1} - k^{21}_{k1}\right) \frac{\phi_{k,r}}{m_{ar}} \\ \vdots \\ \sum_{k=1}^{m} \left(-\lambda_r^2 m^{21}_{kn} - \lambda_r c^{21}_{kn} - k^{21}_{kn}\right) \frac{\phi_{k,r}}{m_{ar}} \end{Bmatrix} = \begin{Bmatrix} T_{1,r} \\ \vdots \\ T_{n,r} \end{Bmatrix}, \tag{A.12}$$

and the division remainder

$$\mathbf{A}^{(0)} = \mathbf{M}_{22}^{-1} \mathbf{M}_{21}, \tag{A.13}$$

which assumes the meaning of a constant term related to the virtually grounded system mass matrix and to the inertial coupling between driving and guided dofs.

References

[1] D. Ewins, Modal Testing: Theory, Practice and Application, Research Study Press Ltd., Baldock, Hertfordshire, England, 2000.

[2] W. Fan, P. Qiao, Vibration-based damage identification methods: A review and comparative study, Struct. Health Monit. 10 (1) (2011) 83–111, http://dx.doi.org/10.1177/1475921710365419.

[3] C. Farrar, S. Doebling, D. Nix, Vibration-based structural damage identification, Phil. Trans. R. Soc. A 359 (1778) (2001) 131–149, http://dx.doi.org/10.1098/rsta.2000.0717.

[4] D. Montalvão, N.M.M. Maia, A. Ribeiro, A review of vibration-based structural health monitoring with special emphasis on composite materials, Shock Vib. Dig. 38 (2006) 295–324.

[5] O. Salawu, Detection of structural damage through changes in frequency: a review, Eng. Struct. 19 (9) (1997) 718–723, http://dx.doi.org/10.1016/S0141-0296(96)00149-6.

[6] A. Ribeiro, On the generalization of the transmissibility concept, in: Proceedings of NATO/ASI Conference on Modal Analysis and Testing, Sesimbra, Portugal, 1998, pp. 757–764, http://dx.doi.org/10.13140/2.1.2538.0801.

[7] R. Sampaio, N. Maia, A. Ribeiro, J. Silva, Damage detection using the transmissibility concept, in: Proceedings of Sixth International Congress on Sound and Vibration, Copenhagen, Denmark, 1999, pp. 2559–2568, http://dx.doi.org/10.13140/2.1.4602.4641.

[8] A. Ribeiro, J. Silva, N. Maia, On the generalisation of the transmissibility concept, Mech. Syst. Signal Process. 14 (1) (2000) 29–35, http://dx.doi.org/10.1006/mssp.1999.1268.

[9] N.M.M. Maia, A.P.V. Urgueira, R.A.B. Almei, Whys and wherefores of transmissibility, in: Vibration Analysis and Control - New Trends and Developments, InTech, 2011, http://dx.doi.org/10.5772/24869.
[10] N.M. Maia, R.A. Almeida, A.P. Urgueira, R.P. Sampaio, Damage detection and quantification using transmissibility, Mech. Syst. Signal Process. 25 (7) (2011) 2475–2483, http://dx.doi.org/10.1016/j.ymssp.2011.04.002.
[11] S. Chesné, A. Deraemaeker, Damage localization using transmissibility functions: A critical review, Mech. Syst. Signal Process. 38 (2) (2013) 569–584, http://dx.doi.org/10.1016/j.ymssp.2013.01.020.
[12] W.-J. Yan, M.-Y. Zhao, Q. Sun, W.-X. Ren, Transmissibility-based system identification for structural health Monitoring: Fundamentals, approaches, and applications, Mech. Syst. Signal Process. 117 (2019) 453–482, http://dx.doi.org/10.1016/j.ymssp.2018.06.053.
[13] L. Cheng, A. Cigada, An analytical perspective about structural damage identification based on transmissibility function, Struct. Health Monit. 19 (1) (2020) 142–155, http://dx.doi.org/10.1177/1475921719838079.
[14] A. Messina, Local diagnoses in modal analysis through additional poles, Mech. Adv. Mater. Struct. (2019) http://dx.doi.org/10.1080/15376494.2019.1614704.
[15] A. Messina, L. Soria, G. Mantriota, Experimental analyses on local diagnoses through additional poles extracted by R-FRFs, Mech. Adv. Mater. Struct. (2019) http://dx.doi.org/10.1080/15376494.2019.1705448.
[16] S. De Carolis, A. Messina, L. Soria, On the estimation process of a particular class of global transmissibility functions: the R-FRFs, Mech. Adv. Mater. Struct. 00 (00) (2021) 000, http://dx.doi.org/10.1080/15376494.2021.1992809.
[17] C. Devriendt, P. Guillaume, The use of transmissibility measurements in output-only modal analysis, Mech. Syst. Signal Process. 21 (7) (2007) 2689–2696, http://dx.doi.org/10.1016/j.ymssp.2007.02.008.
[18] C. Devriendt, P. Guillaume, Identification of modal parameters from transmissibility measurements, J. Sound Vib. 314 (1) (2008) 343–356, http://dx.doi.org/10.1016/j.jsv.2007.12.022.
[19] W. Weijtjens, G. De Sitter, C. Devriendt, P. Guillaume, Operational modal parameter estimation of MIMO systems using transmissibility functions, Automatica 50 (2) (2014) 559–564, http://dx.doi.org/10.1016/j.automatica.2013.11.021.
[20] C. Devriendt, G. De Sitter, P. Guillaume, An operational modal analysis approach based on parametrically identified multivariable transmissibilities, Mech. Syst. Signal Process. 24 (5) (2010) 1250–1259, http://dx.doi.org/10.1016/j.ymssp.2009.02.015, Special Issue: Operational Modal Analysis.
[21] W. Heylen, S. Lammens, P. Sas, Modal Analysis Theory and Testing, Katholieke Universiteit Leuven, Departement Werktuigkunde, Leuven, Belgium, 1997.
[22] R. Brincker, P.H. Kirkegaard, Special issue on operational modal analysis, Mech. Syst. Signal Process. 24 (5) (2010) 1209–1212, http://dx.doi.org/10.1016/j.ymssp.2010.03.005, Special Issue: Operational Modal Analysis.
[23] L. Zhang, R. Brincker, P. Andersen, An overview of operational modal analysis: Major development and issues, in: Proceedings of the 1st International Operational Modal Analysis Conference, IOMAC 2005, 2005.
[24] G. James, T. Carne, J. Laufer, The natural excitation technique (NExT) for modal parameter extraction from operating structures, J. Anal. Exp. Modal Anal. 10 (1995).
[25] R. Brincker, C. Ventura, Introduction to operational modal analysis, 2015, pp. 1–360, http://dx.doi.org/10.1002/9781118535141.
[26] C. Rainieri, G. Fabbrocino, Operational modal analysis of civil engineering structures, an introduction and a guide for applications, 2014, http://dx.doi.org/10.1007/978-1-4939-0767-0.
[27] F. Shen, M. Zheng, D. Feng Shi, F. Xu, Using the cross-correlation technique to extract modal parameters on response-only data, J. Sound Vib. 259 (5) (2003) 1163–1179, http://dx.doi.org/10.1006/jsvi.2002.5203.
[28] E. Parloo, Application of Frequency-Domain System Identification Techniques in the Field of Operational Modal Analysis (Ph.D. thesis), Dept. of Mechanical Engineering, Vrije Universiteit Brussel, Belgium, 2003.
[29] P. Fernández, P. Reynolds, M. López-Aenlle, Scaling mode shapes in output-only systems by a consecutive mass change method, Exp. Mech. 51 (6) (2011) 995–1005, http://dx.doi.org/10.1007/s11340-010-9400-0.
[30] M. Khatibi, M. Ashory, A. Malekjafarian, R. Brincker, Mass–stiffness change method for scaling of operational mode shapes, Mech. Syst. Signal Process. 26 (2012) 34–59, http://dx.doi.org/10.1016/j.ymssp.2011.07.012.
[31] R. Brincker, Some elements of operational modal analysis, Shock Vib. 2014 (2014) http://dx.doi.org/10.1155/2014/325839.
[32] P. Guillaume, P. Verboven, S. Vanlanduit, H. Van der Auweraer, B. Peeters, A poly-reference implementation of the least-squares complex frequency-domain estimator, in: Proceedings of IMAC, Vol. 21, 2003.
[33] A. Edelman, H. Murakami, Polynomial roots from companion matrix eigenvalues, Math. Comp. 64 (210) (1995) 763–776, http://dx.doi.org/10.1090/S0025-5718-1995-1262279-2.
[34] P. Andersen, Identification of Civil Engineering Structures Using Vector ARMA Models (Ph.D. thesis), University of Aalborg, Aalborg, 2003.
[35] P. Guillaume, R. Pintelon, J. Schoukens, Nonparametric frequency response function estimators based on nonlinear averaging techniques, IEEE Trans. Instrum. Meas. 41 (6) (1992) 739–746, http://dx.doi.org/10.1109/19.199393.